

Construction of AgCl/Bi₂WO₆ heterojunction for effective removal of RhB dye

Y. T. Zhang^a, D. Y. Wang^a, X. Luo^a, K. Lei^a, L. J. Mao^a, Y. J. Duan^a, X. H. Zeng^a,
G. J. Wan^b, Q. Zhao^{c,*}, Y. Sun^{a,*}

^a*School of Mechanical Engineering, Chengdu University, Chengdu, 610106, China*

^b*School of Materials Science and Engineering, Southwest Jiaotong University, Chengdu, 611756, China*

^c*School of Chemical Engineering, Sichuan University, Chengdu, 610065, China*

Flower-like Bi₂WO₆ microspheres were prepared by a facile hydrothermal method, and AgCl/Bi₂WO₆ heterojunction was successfully synthesized by in-situ precipitation method. The samples were characterized by X-ray diffraction (XRD), X-ray photoelectron spectroscopy (XPS), scanning electron microscopy (SEM) and UV-vis diffuse reflectance spectroscopy (DRS). The effect of AgCl loading in AgCl/Bi₂WO₆ composites on the degradation of Rhodamine B (RhB) was also investigated. When the mass ratio of AgCl to Bi₂WO₆ was 4:1, AgCl/Bi₂WO₆ composites exhibited the highest photocatalytic degradation efficiency of 87.9% within 30 min, which could be attributed to the construction of heterojunction structure that effectively promoted the separation of photogenerated electron-hole pairs.

(Received January 11, 2024; Accepted April 11, 2024)

Keywords: Flower-like Bi₂WO₆, AgCl/Bi₂WO₆, heterojunction, Photocatalysis

1. Introduction

With the development of industry, the problem of water pollution has become increasingly serious. In recent years, photocatalytic technology is recognized as one of the most effective strategies for the removal of organic pollutants from wastewater [1]. Multi-metal oxide semiconductors such as Bi₂WO₆, BiVO₄, Bi₂MoO₆ have been broadly studied in many fields owing to their advantages including facile preparation, low price and stable properties [2-4]. Among them, Bi₂WO₆, a n-type semiconductor with suitable bandgap structure, is regarded as a promising visible-light-driven photocatalyst. However, the photocatalytic performance of Bi₂WO₆ is limited by the poor response to visible light and low separation efficiency of electron-holes pair. To solve these issues, element doping [5], noble metal deposition [6], and heterojunction construction [7] have been used to improve the photocatalytic activity. Recently, the localized surface plasmon resonance (LSPR) effect of Ag/AgCl photocatalyst has been utilized to remove organic pollutants owing to the strong absorption of visible light [8]. The loading of Ag/AgCl onto other photocatalysts to form heterostructure is an effective way to separate charge carriers, such as Ag/AgCl/TiO₂ [9], Ag/AgCl/ZnTiO₃ [10], Ag/AgCl/Bi₂O₃/BiFeO₃ [11].

* Corresponding author: sunyan@cdu.edu.cn
<https://doi.org/10.15251/DJNB.2024.192.571>

Furthermore, the combination of Ag/AgCl with flower-like semiconductors, such as Ag/AgCl/WO₃ [12] and Ag/AgCl/BiOCl [13], can increase the active sites and then greatly improve the photocatalytic activity.

In this study, an in-situ precipitation method was employed to synthesize AgCl/Bi₂WO₆ heterojunction photocatalyst, in which a self-assembled Bi₂WO₆ microspheres was fabricated using a hydrothermal method. The photocatalytic activity of the catalysts was evaluated by degrading Rhodamine B (RhB) under irradiation. In addition, the trapping experiments were carried out to explore the photocatalytic degradation mechanism.

2. Experimental

2.1. Preparation of AgCl/Bi₂WO₆ catalyst

2 mmol of Na₂WO₄·2H₂O and 4 mmol of Bi(NO₃)₃·5H₂O were ultrasonically dissolved in 30 mL and 40 mL of deionized water, respectively. Subsequently, the Na₂WO₄ solution was added to the prepared Bi(NO₃)₃ solution under vigorous stirring for 1 h. Then the suspension was transferred into a 100 mL Teflon-sealed autoclave and heated at 180 °C for 24 h. Finally, the product was obtained after repeated washing with deionized water and ethanol.

The AgCl/ Bi₂WO₆ product was prepared using an in-situ precipitation method. Briefly, 1mmol of KCl and 1mmol of AgNO₃ were dissolved in 20 mL distilled water, respectively. A certain amount of Bi₂WO₆ were dispersed in the AgNO₃ solution by stirring for 30 min, and then the KCl solution was added dropwise into the mixture with stirring. The finally products with different mass ratios of AgCl to Bi₂WO₆ (1:4, 1:1, 4:1) were washed with deionized water and dried at 60 °C for 8h.

2.2. Characterization

The crystal structure of the samples was characterized using X-ray diffraction (XRD, Ultima IV). The morphology and microstructure were examined by field emission scanning electron microscopy (SEM, ZEISS Gemini 300). The surface elemental compositions and corresponding chemical states of prepared samples were performed by X-ray photoelectron spectroscopy (XPS, K-Alpha). Using BaSO₄ as a reflectance, UV-vis diffuse reflectance spectra (UV-vis DRS) were carried out on a TU-1901 spectrophotometer.

2.3. Photocatalytic activity

Photocatalytic activity of the samples was evaluated via the degradation of RhB dye under simulated solar light irradiation using a 500 W xenon lamp (AM1.5, 100 mW/cm²). 100 mg of the photocatalyst was added to 100 mL of RhB solution (10 mg/L). Before illumination, the suspension was stirred for 30 min in the dark to reach the adsorption–desorption equilibrium. 5 mL suspension was sampled at 5 min intervals and centrifuged to remove photocatalyst particles. The concentration of RhB was analyzed via a UV-vis spectrophotometer at the absorption peak of 554 nm.

2.4. Active species trapping test

To explore the main active species for the degradation of RhB dye, tertiary butanol (TBA, 10 mM), triethanolamine (TEOA, 1 mM), and 1,4-benzoquinone (BQ, 1 mM) were used as scavengers to capture hydroxyl radicals ($\cdot\text{OH}$), holes (h^+), and superoxide radicals ($\cdot\text{O}_2^-$), respectively. The detailed experimental procedure was similar to that of the photocatalytic activity test.

3. Results and discussion

The XRD patterns of AgCl, Bi_2WO_6 , and the AgCl/ Bi_2WO_6 composites with different Bi_2WO_6 contents were displayed in Fig. 1a. The characteristic peaks at 28.4° , 32.9° , 47.1° , 56.0° , 58.7° correspond to (131), (200), (202), (331) and (262) crystal planes of Bi_2WO_6 (JCPDS# 39-0256). The characteristic peaks of AgCl at 27.8° , 32.2° , 46.2° , 54.8° , 57.4° and 67.4° are ascribed to the (111), (200), (220), (311), (222) and (400) planes (JCPDS# 31-1238), respectively. In the XRD patterns of the AgCl/ Bi_2WO_6 composites, all peaks can be assigned to AgCl and Bi_2WO_6 and no extra peaks appear, which indicates that the AgCl/ Bi_2WO_6 composites were successfully synthesized. Moreover, with the increase of AgCl content, the peak intensity of AgCl in composites increases while the peak intensity of Bi_2WO_6 continually decreases.

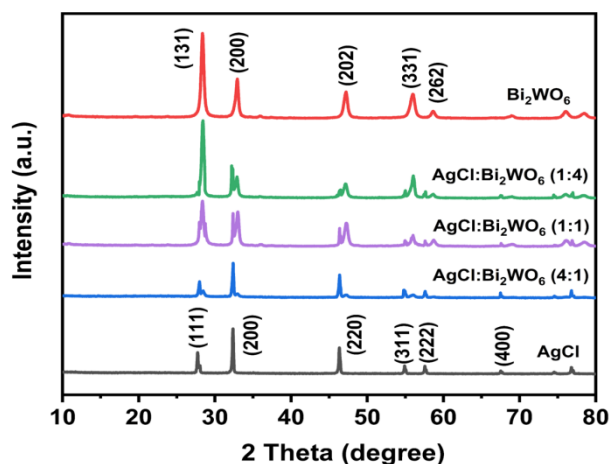


Fig. 1. XRD patterns of the as-prepared samples.

Fig. 2 shows the SEM images of AgCl, Bi_2WO_6 , and AgCl/ Bi_2WO_6 composites. It can be seen from Fig. 2a-b that Bi_2WO_6 shows a three-dimensional (3D) flower-like hierarchical microstructure with the diameter of about 3-4 μm , which is self-assembled from a large number of 2D nanosheets. Fig. 2c shows that the fabricated AgCl sample is composed of irregular particles with smooth surface and the size is around 1-2 μm . For AgCl/ Bi_2WO_6 composites (Fig. 2d-f), it is clear that the coupling of AgCl did not change the overall morphology of Bi_2WO_6 . When the AgCl content gradually increases, more AgCl nanoparticles can be observed, which are aggregated around the Bi_2WO_6 microspheres. Fig. 2g is the elemental mapping images of AgCl/ Bi_2WO_6 (4:1)

sample, which further confirms that the sample contains a uniform distribution of Bi, W, O, Ag and Cl elements.

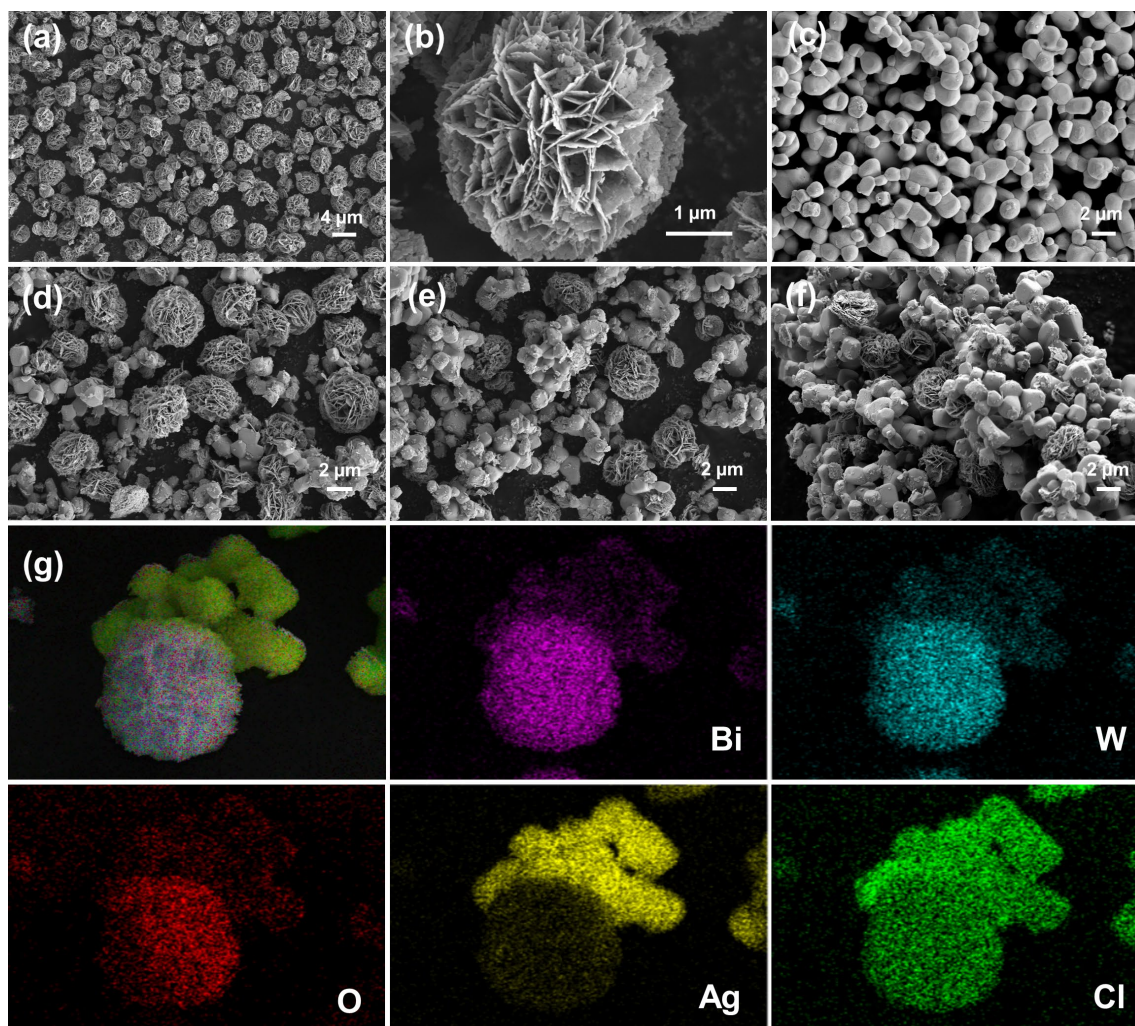


Fig. 2. SEM images of (a-b) Bi_2WO_6 , (c) AgCl , (d) $\text{AgCl}/\text{Bi}_2\text{WO}_6$ (1:4), (e) $\text{AgCl}/\text{Bi}_2\text{WO}_6$ (1:1), (f) $\text{AgCl}/\text{Bi}_2\text{WO}_6$ (4:1) and (g) elemental mapping of $\text{AgCl}/\text{Bi}_2\text{WO}_6$ (4:1) sample.

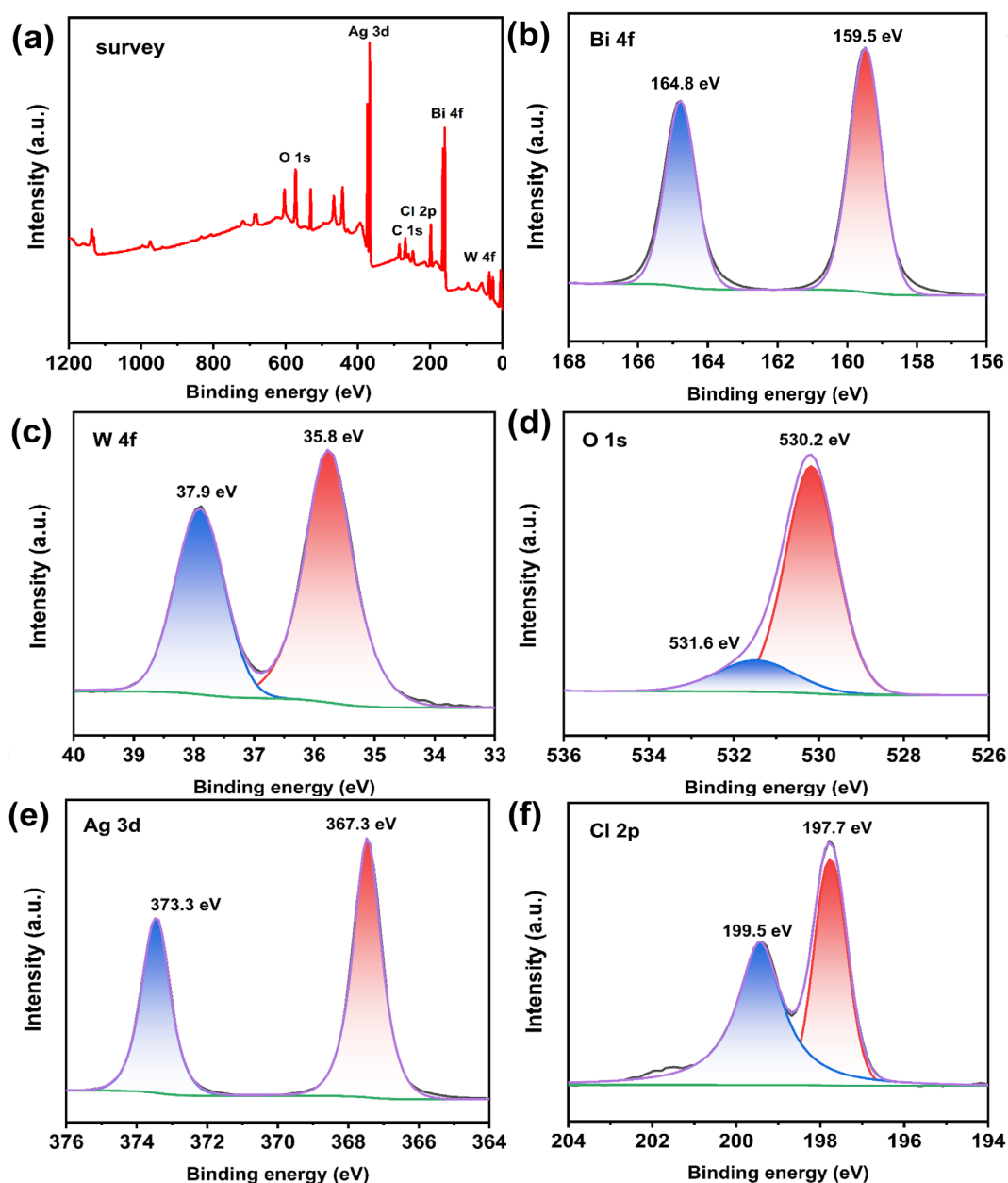


Fig. 3. XPS patterns of AgCl/Bi₂WO₆ (4:1) sample: (a) survey spectrum, (b) Bi 4f, (c) W 4f, (d) O 1s, (e) Ag 3d and (f) Cl 2p.

The XPS survey spectrum (Fig. 3a) indicates that AgCl/Bi₂WO₆ is mainly composed of W, O, Cl Bi and Ag elements. For the Bi 4f spectrum (Fig. 3b), two peaks at 159.5 and 164.8 eV correspond to Bi 4f_{7/2} and Bi 4f_{5/2}, certifying the Bi³⁺ ions in the sample [14]. Fig. 3c is XPS spectrum of W 4f and the peaks at 35.8 and 37.9 eV are assigned to W 4f_{7/2} and W 4f_{5/2} for W⁶⁺ [15]. In Fig. 3d, the O 1s spectrum can be divided into two peaks of 530.2 and 531.6 eV, corresponding to the lattice oxygen (Bi–O, W–O) and surface hydroxyl groups, respectively [16]. In Fig. 3e, the peaks at the binding energy of 367.3 and 373.3 eV are primarily assigned to Ag 3d_{5/2} and Ag 3d_{3/2}, which reveals the existence of Ag⁺ in the samples [17]. As displayed in Fig. 3f, the

peaks at binding energies of 197.7 and 199.5 eV are ascribed to Cl 2p_{3/2} and Cl 2p_{1/2}, suggesting the chemical state of Cl⁻ [18].

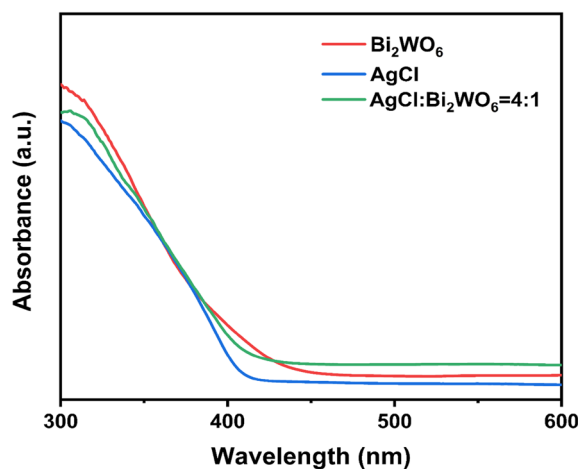


Fig. 4. UV-vis DRS spectra of Bi_2WO_6 , AgCl and $\text{AgCl}/\text{Bi}_2\text{WO}_6$ (4:1).

The UV-vis diffuse reflectance spectra of AgCl , Bi_2WO_6 , and $\text{AgCl}/\text{Bi}_2\text{WO}_6$ (4:1) are shown in Fig. 4. The absorption edge of AgCl is at approximately 420 nm, whereas that of Bi_2WO_6 is at about 438 nm. Therefore, the introduction of Bi_2WO_6 in $\text{AgCl}/\text{Bi}_2\text{WO}_6$ can extend the light absorption to the visible light region, leading to more photogenerated electron-hole pairs.

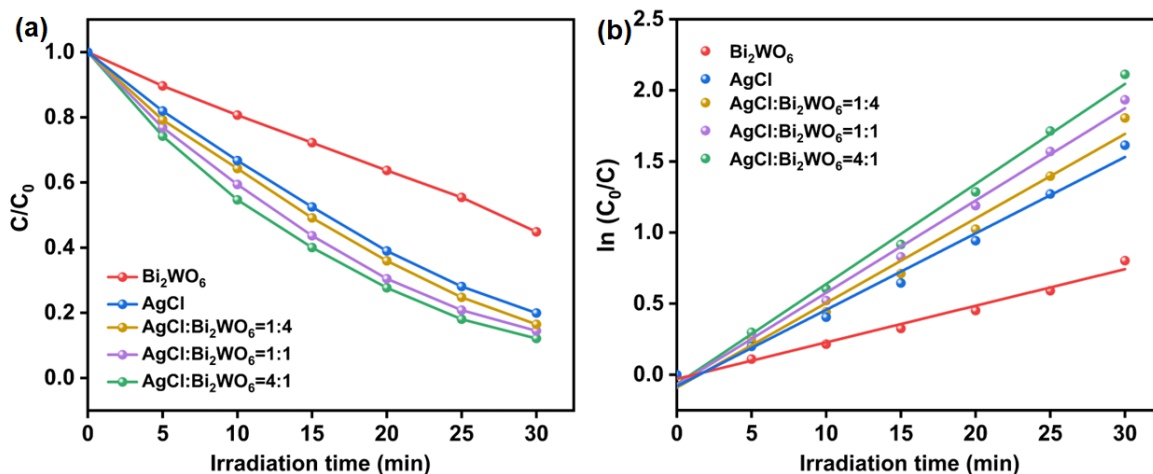


Fig. 5. (a) Photocatalytic activity of all samples; (b) corresponding pseudo-first order kinetics.

The photocatalytic activity of all samples was evaluated by RhB degradation. As shown in Fig. 5a, the removal efficiency of pure AgCl is 80.1 % within 30 min, while the removal efficiency of pure Bi_2WO_6 is only 55.2 %. Obviously, all $\text{AgCl}/\text{Bi}_2\text{WO}_6$ composites exhibit higher photocatalytic activities than AgCl and Bi_2WO_6 . With the increase of AgCl content, the photocatalytic activity of the composites is gradually improved. When the mass ratio of AgCl to

Bi_2WO_6 is 4:1, the highest degradation efficiency reaches 87.9 % within 30 min. This can be explained by the formation of heterojunction structure that accelerates the separation and transfer of photogenerated electron-hole pairs and suppresses the recombination of charge carriers, thus improving the photocatalytic activity. Additionally, the degradation rate of RhB can be fitted by pseudo-first-order kinetic model. As seen in Fig. 5b, the degradation rate of all catalysts follows the first-order reaction kinetics. The reaction rate constant of $\text{AgCl}/\text{Bi}_2\text{WO}_6$ (4:1) sample is 1.31 and 2.74 times that of AgCl (0.0537 min^{-1}) and Bi_2WO_6 (0.0257 min^{-1}), respectively.

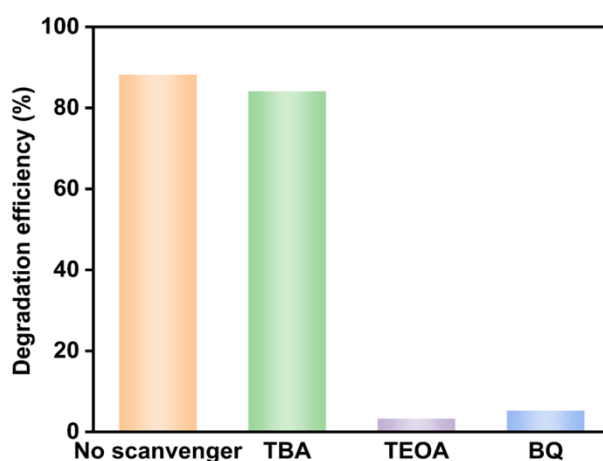


Fig. 6. Trapping experiments of $\text{AgCl}/\text{Bi}_2\text{WO}_6$ (4:1) for photocatalytic degradation of RhB.

The trapping experiments were employed to detect the main active species during the photocatalytic degradation process, using TBA, BQ, and TEOA to capture hydroxyl radicals ($\cdot\text{OH}$), superoxide radicals ($\cdot\text{O}_2^-$), and holes (h^+), respectively. As shown in Fig. 6, when TEOA and BQ are added in RhB solution, the degradation efficiency dramatically decreases to 3.3 % and 5.3 %, respectively, which indicates that h^+ and $\cdot\text{O}_2^-$ are the main active species in the photocatalytic reaction.

4. Conclusions

In this work, self-assembled Bi_2WO_6 microspheres were synthesized by hydrothermal method and $\text{AgCl}/\text{Bi}_2\text{WO}_6$ composites were synthesized via an in-situ precipitation method. The photocatalytic experimental results indicated that all the as-prepared $\text{AgCl}/\text{Bi}_2\text{WO}_6$ composites exhibited superior photocatalytic activity under simulated solar-light irradiation compared with AgCl and Bi_2WO_6 . The highest degradation efficiency of 87.9 % was achieved when the mass ratio of AgCl to Bi_2WO_6 was 4:1, which was mainly ascribed to the formation of heterojunction structure that effectively inhibited the recombination of photogenerated electron-hole pairs.

Acknowledgments

This research was supported by Sichuan University-Suining City Cooperation Science and Technology Project "Methods and Dynamics for Increasing the Densification of Electroplated Tin Layer" (NO. 2021CDSN-06).

References

- [1] Z. Zheng, S. Tian, Y. Feng, S. Zhao, X. Li, S. Wang, Z. He, *Chinese Journal of Catalysis* 54, 88-136 (2023); [https://doi.org/10.1016/S1872-2067\(23\)64536-X](https://doi.org/10.1016/S1872-2067(23)64536-X)
- [2] B. Miao, Y. Chu, X. Zheng, H. Su, *Materials Science in Semiconductor Processing* 125, 105636 (2021); <https://doi.org/10.1016/j.mssp.2020.105636>
- [3] Z. Zhu, S. Wan, Y. Zhao, Y. Qin, X. Ge, Q. Zhong, Y. Bu, *Nano Select* 2(2), 187-215 (2021); <https://doi.org/10.1002/nano.202000127>
- [4] R. Srinivasan, E. Elaiyappillai, S. Anandaraj, B. k. Duvaragan, P. M. Johnson, *Journal of Electroanalytical Chemistry* 861, 113972 (2020); <https://doi.org/10.1016/j.jelechem.2020.113972>
- [5] Z. Yang, H. Zeng, J. Xiong, D. Peng, S. Liu, *Colloids and Surfaces A: Physicochemical and Engineering Aspects* 675, 132035 (2023); <https://doi.org/10.1016/j.colsurfa.2023.132035>
- [6] S. Zhang, W. Pu, A. Chen, Y. Xu, Y. Wang, C. Yang, J. Gong, *Journal of hazardous materials* 384, 121478 (2020); <https://doi.org/10.1016/j.jhazmat.2019.121478>
- [7] B. Zhao, N. Shao, X. Chen, J. Ma, Y. Gao, X. Chen, *Colloids and Surfaces A: Physicochemical and Engineering Aspects* 663, 131072 (2023); <https://doi.org/10.1016/j.colsurfa.2023.131072>
- [8] H. Lv, Y. Duan, X. Zhou, G. Liu, X. Wang, Y. Wang, M. Yuan, Q. Meng, C. Wang, *Catalysis Science & Technology* 10(24), 8230-8239 (2020); <https://doi.org/10.1039/D0CY01293A>
- [9] M. Maneshi, P. Cerruti, A. Moeini, M. Davoodi, *Advanced Powder Technology* 33(11), 103808 (2022); <https://doi.org/10.1016/j.apt.2022.103808>
- [10] M. Padervand, S. Ghasemi, S. Hajiahmadi, B. Rhimi, Z. G. Nejad, S. Karima, Z. Shahsavari, C. Wang, *Applied Catalysis A: General* 643, 118794 (2022); <https://doi.org/10.1016/j.apcata.2022.118794>
- [11] Y. Li, W. Yin, M. Li, J. Zhang, L. Chen, *Journal of Environmental Chemical Engineering* 10(2), 107280 (2022); <https://doi.org/10.1016/j.jece.2022.107280>
- [12] B. Ma, J. Guo, W. L. Dai, K. Fan, *Applied Catalysis B: Environmental* 123, 193-199 (2012); <https://doi.org/10.1016/j.apcatb.2012.04.029>
- [13] S. Zhao, Y. Zhang, Y. Zhou, K. Qiu, C. Zhang, J. Fang, X. Sheng, *Journal of Photochemistry and Photobiology A: Chemistry* 350, 94-102 (2018); <https://doi.org/10.1016/j.jphotochem.2017.09.070>
- [14] Y. Q. Liu, Y. L. Xu, D. J. Zhong, H. Y. Yao, Y. D. Zeng, N. B. Zhong, H. Luo, *Colloids and Surfaces A: Physicochemical and Engineering Aspects* 612, 125941 (2021); <https://doi.org/10.1016/j.colsurfa.2020.125941>
- [15] G. Chen, Y. Wang, Q. Shen, X. Xiong, S. Ren, G. Dai, C. Wu, *Ceramics International* 46, 21304-21310 (2020); <https://doi.org/10.1016/j.ceramint.2020.05.224>

- [16] X. Wang, Z. C. Guan, P. Jin, Y. Y. Tang, G. L. Song, G. K. Liu, R. G. Du, *Corrosion Science* 157, 247-255 (2019); <https://doi.org/10.1016/j.corsci.2019.05.034>
- [17] Y. Wang, H. Yang, X. Sun, H. Zhang, T. Xian, *Materials Research Bulletin* 124, 110754 (2020); <https://doi.org/10.1016/j.materresbull.2019.110754>.
- [18] N. R. Barveen, T. J. Wang, Y. H. Chang. *Chemical Engineering Journal* 423, 130191 (2021); <https://doi.org/10.1016/j.cej.2021.130191>
- [19] Y. Tan, Y. Zhou, Y. Deng, H. Tang, H. Zou, Y. Xu, J. Li, *Colloids and Surfaces A: Physicochemical and Engineering Aspects*, A 622, 126699 (2021); <https://doi.org/10.1016/j.colsurfa.2021.126699>
- [20] Y. Wang, M. Zhang, J. Li, H. Yang, J. Gao, G. He, Z. Sun, *Applied Surface Science* 476, 84-93 (2019); <https://doi.org/10.1016/j.apsusc.2019.01.086>